PROCEEDINGS OF SCIENCE

New result on the search for the $K^+ \to \pi^+ \nu\bar{\nu}$ decay at the NA62 experiment at CERN

Radoslav Marchevski *

CERN, Geneva, Switzerland

E-mail: rmarchev@cern.ch

The ultra-rare $K^+ \to \pi^+ \nu\bar{\nu}$ decay benefits from a precisely predicted branching ratio in the SM $BR(K^+ \to \pi^+ \nu\bar{\nu}) = (8.4 \pm 1.0) \times 10^{-11}$, being almost free from theoretical uncertainties, and most importantly from a very high sensitivity to a variety of beyond-the-standard-model scenarios, making it one of the best candidates to reveal indirect effects of new physics in the flavour sector. The NA62 experiment at the CERN SPS, designed to measure the branching ratio of $K^+ \to \pi^+ \nu\bar{\nu}$ with a decay-in-flight technique, collected data in 2016-2018. New results from the analysis of 2018 data, the largest data set so far collected, will be presented. The result will represent the most accurate measurement so far achieved of this ultra-rare decay.

40th International Conference on High Energy physics - ICHEP2020
July 28 - August 6, 2020
Prague, Czech Republic (virtual meeting)

*On behalf of the NA62 Collaboration: R. Aliberti, F. Ambrosino, R. Ammendola, B. Angelucci, A. Antonelli, G. Anzivino, R. Arcidiacono, T. Bache, A. Baeva, D. Baigarashev, M. Barbanera, J. Bernhard, A. Biagioni, L. Bician, C. Biino, A. Bizzeti, T. Blazek, B. Bloch-Devaux, V. Bonaiuto, M. Boretto, M. Bragadireanu, D. Britton, F. Brizioli, M.B. Brunetti, D. Bryman, F. Bucci, T. Capussela, J. Carmignani, A. Ceccucci, P. Cenci, V. Cerny, C. Cerri, B. Checcucci, A. Conovaloff, P. Cooper, E. Cortina Gil, M. Corvino, F. Costantini, A. Cotta Ramusino, D. Coward, G. D'Agostini, J. Dainton, P. Dalpiaz, H. Danielsson, N. De Simone, D. Di Filippo, L. Di Lella, N. Doble, B. Dobrich, F. Duval, V. Duk, D. Emelyanov, J. Engelfried, T. Enik, N. Estrada-Tristan, V. Falaleev, R. Fantechi, V. Fascianelli, L. Federici, S. Fedotov, A. Filippi, M. Fiorini, J. Fry, J. Fu, A. Fucci, L. Fulton, E. Gamberini, L. Gatignon, G. Georgiev, S. Ghinescu, A. Gianoli, M. Giorgi, S. Giudici, F. Gonnella, E. Goudzovski, C. Graham, R. Guida, E. Gushchin, F. Hahn, H. Heath, J. Henshaw, E.B. Holzer, T. Husek, O. Hutanu, D. Hutchcroft, L. Iacobuzio, E. Iacopini, E. Imbergamo, B. Jenninger, J. Jerhot, R.W. Jones, K. Kampf, V. Kekelidze, S. Kholodenko, G. Khoriauli, A. Khotyantsev, A. Kleimenova, A. Korotkova, M. Koval, V. Kozhuharov, Z. Kucerova, Y. Kudenko, J. Kunze, V. Kurochka, V. Kurshetsov, G. Lanfranchi, G. Lamanna, E. Lari, G. Latino, P. Laycock, C. Lazzeroni, M. Lenti, G. Lehmann Miotto, E. Leonardi, P. Lichard, L. Litov, R. Lollini, D. Lomidze, A. Lonardo, P. Lubrano, M. Lupi, N. Lurkin, D. Madigozhin, I. Mannelli, A. Mapelli, F. Marchetto, R. Marchevski, S. Martellotti, P. Massarotti, K. Massri, E. Maurice, M. Medvedeva, A. Mefodev, E. Menichetti, E. Migliore, E. Minucci, M. Mirra, M. Misheva, N. Molokanova, M. Moulson, S. Movchan, M. Napolitano, I. Neri, F. Newson, A. Norton, M. Noy, T. Numao, V. Obraztsov, A. Ostankov, S. Padolski, R. Page, V. Palladino, A. Parenti, C. Parkinson, E. Pedreschi, M. Pepe, M. Perrin-Terrin, L. Peruzzo, P. Petrov, Y. Petrov, F. Petrucci, R. Piandani, M. Piccini, J. Pinzino, I. Polenkevich, L. Pontisso, Yu. Potrebenikov, D. Protopopescu, M. Raggi, A. Romano, P. Rubin, G. Ruggiero, V. Ryjov, A. Salamon, C. Santoni, G. Saracino, F. Sargeni, S. Schuchmann, V. Semenov, A. Sergi, A. Shaikhiev, S. Shkarovskiy, D. Soldi, V. Sugonyaev, M. Sozzi, T. Spadaro, F. Spinella, A. Sturgess, J. Swallow, S. Trilov, P. Valente, B. Velghe, S. Venditti, P. Vicini, R. Volpe, M. Vormstein, H. Wahl, R. Wanke, B. Wrona, O. Yushchenko, M. Zamkovsky, A. Zinchenko.

PoS(ICHEP2020)398

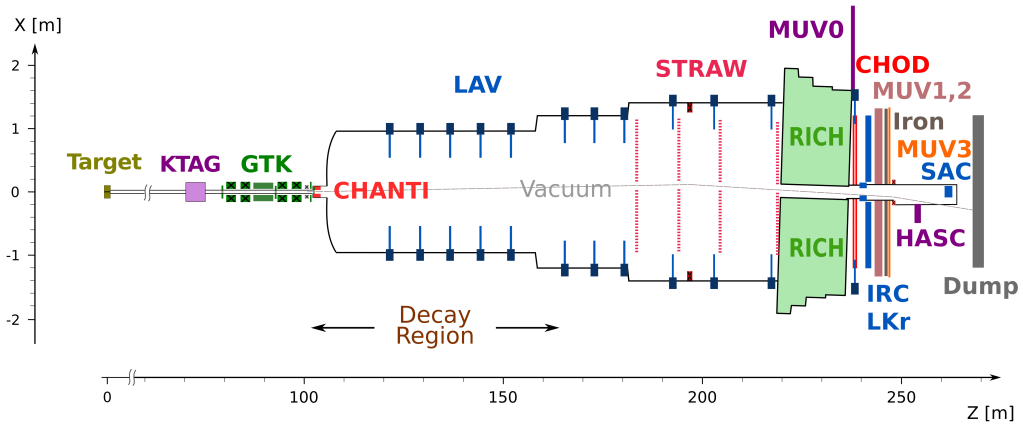

Figure 1: Schematic layout of the NA62 experiment in the xz plane

1. Introduction

The $K^+ \to \pi^+ \nu\bar{\nu}$ decay is a flavour changing neutral current process proceeding through box and electroweak penguin diagrams. The process is very rare, due to quadratic GIM mechanism and strong Cabibbo suppression. The dominant contribution comes from the short-distance top quark loop, with a small charm quark contribution and long-distance corrections. The hadronic matrix element relevant for the $K^+ - \pi^+$ transition can be extracted experimentally from $K^+ \to l^+\pi^0\nu_l$ decays after correcting for isospin. This eliminates important theoretical uncertainties and makes the $K^+ \to \pi^+\nu\bar{\nu}$ decay very clean theoretically and sensitive to physics beyond the Standard Model (SM), probing the highest mass scales among the rare meson decays [1–6]. The SM prediction using elements of the Cabibbo-Kobayashi-Maskawa (CKM) matrix extracted from tree-level processes [7, 8] is

$$BR(K^+ \to \pi\nu\bar{\nu}) = (8.4 \pm 1.0) \times 10^{-11}. \quad (1)$$

The knowledge of the external inputs dominate the uncertainties on the prediction.

2. NA62 beam and detector

The fixed-target NA62 experiment exploits a 400 GeV/c primary SPS proton beam. The beam impinges on a beryllium target producing secondary particles, of which the kaon component is 6%. A 100 m long beam line selects, collimates, focuses and transports charged particles of (75.0±0.8) GeV/c momentum to the evacuated fiducial decay volume.

The NA62 experimental apparatus is shown in Figure 1. The KTAG is a differential Cherenkov detector filled with Nitrogen placed in the beam to identify and timestamp kaons. It is followed by the Gigatracker (GTK) detector, composed of three silicon pixel stations of 6×3 cm^2 surface exposed to the full 750 MHz beam rate. The GTK is used to timestamp and measure the momentum of the beam particles before entering the vacuum region downstream. The CHANTI detector, placed after the Gigatracker, tags hadronic beam-detector interactions in the last GTK station. Downstream, the magnetic spectrometer, made of four straw chambers and a dipole magnet between the second and third chamber is used to measure the momentum of the charged K^+ decay particles. A 17 m long

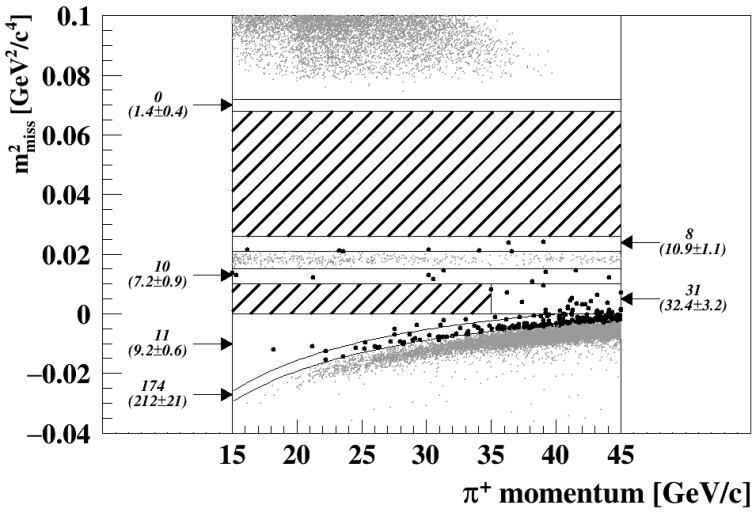

Figure 2: Reconstructed m^2_{miss} as a function of π^+ momentum after the complete signal selection. The background regions where the well-reconstructed peaking backgrounds can be found are depicted by the small grey dots. The regions with the solid black dots neighbouring the background regions are background validation regions, kept masked until the analysis is complete. The numbers next to those regions are the expected number of background events (in brackets) and the observed number (without brackets). The signal regions are indicated by the hatched rectangles: Region 1 (R1) is defined by a (15-35 GeV/c) momentum range and m^2_{miss} between 0 and 0.01 GeV$^2/c^4$; Region 2 (R2) is defined by a (15-45 GeV/c) momentum range and m^2_{miss} between 0.026 and 0.068 GeV$^2/c^4$. R1 and R2 are kept masked until the completion of the analysis.

RICH counter filled with Neon gas is used to separate π^+, μ^+ and e$^+$. The time of charged particles is measured both with the RICH and with an array of scintillators (CHOD) located downstream of the RICH. Two hadronic calorimeters (MUV1 and MUV2) and a fast scintillator array (MUV3) provide further separation between π^+ and μ^+. A set of photons vetoes (LAVs, LKr, IRC, SAC) hermetically cover angles up to 50 mrad to reject extra electromagnetic activity. A detailed description of the apparatus can be found in the NA62 beam and detector paper [9].

3. The $K^+ \to \pi^+\nu\bar{\nu}$ analysis

The experimental signature of the $K^+ \to \pi^+\nu\bar{\nu}$ decay consists of a K^+ with momentum p_K in the initial state, a π^+ with momentum p_π and missing energy in the final state. The kinematic variable used to discriminate between the signal and background K^+ decays is the squared missing mass $m^2_{\text{miss}} = (p_K - p_\pi)^2$. This variable is used to discriminate between the signal and the other peaking K^+- decay backgrounds. The criteria to select $K^+ \to \pi^+\nu\bar{\nu}$ decays include the presence of a downstream charged particle and a K^+ beam particle and are listed below.

Events with a single-track decay topology are selected using the downstream detectors STRAW, CHOD and RICH. The downstream charged track measured by the STRAW detector must be associated both in space and time with a pair of signals in the CHOD and a reconstructed ring in the RICH, where the time is measured with 100 ps resolution. This downstream charged track is

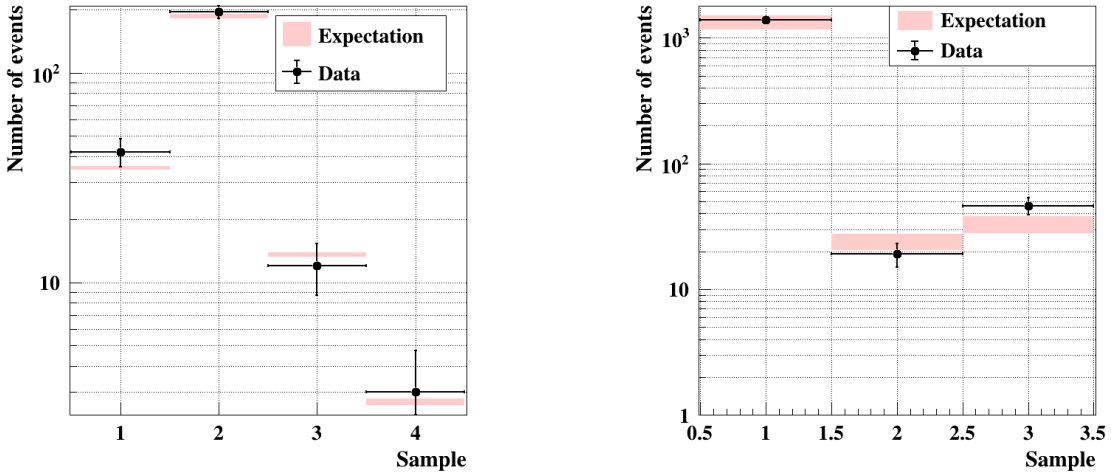

Figure 3: Left: Comparison between expected and observed number of events for four $K^+ \to \pi^+\pi^-e^+\nu$ validation samples. Those samples, enriched of $K^+ \to \pi^+\pi^-e^+\nu$ events, are selected by inverting charge multiplicity rejection cuts or the charge of the downstream particle. **Right:** Comparison between expected and observed number of events for three upstream validation samples. Those samples, enriched of upstream background events, are selected by inverting the BDT criteria used to reject upstream background and selecting two different $m^2_{\rm miss}$ regions: $0.0 < m^2_{\rm miss} < 0.01$ and $0.026 < m^2_{\rm miss} < 0.068$, corresponding to signal regions R1 and R2; $m^2_{\rm miss} < -0.05$.

associated to an in-time K^+ in the KTAG detector. The K^+ track is reconstructed and time-stamped in the GTK detector. The kaon decay vertex is defined as the mid-point of the closest distance of approach of the GTK and STRAW tracks. The kaon decays within a 50 m long fiducial region beginning 10 m downstream of the last GTK station (GTK3) are selected.

The downstream track is identified as a π^+ by two complementary methods using different detectors: a multivariate analysis with Boosted Decision Trees (BDT) using energy deposition, energy sharing and shower shape profiles in the electromagnetic (LKr) and hadronic calorimeters (MUV1/2), as well as signals from the muon veto (MUV3); a cut-based approach using the particle mass reconstructed by the RICH detector and a track-driven likelihood discriminant for $\pi/\mu/e$ separation. Additionally a photon and multi-charged particle rejection is applied based on information in all electromagnetic calorimeters (LKr, LAV, SAC and IRC) and the charged hodoscope (CHOD). The $m^2_{\rm miss}$ distribution after the complete signal selection is shown in Figure 2.

The 2018 data set is divided into two periods with dedicated selections, before (S1) and after (S2) the installation of a new collimator, corresponding to 20% and 80% of the 2018 data set, respectively. The S1 sample is obtained by applying the same selection as for the 2017 data described in detail in [11], exept for an optimized fiducial volume (FV) definition and a momentum range extension to 45 GeV/c in R2. Major improvements are made possible for the S2 sample by the installation of a collimator with larger outer dimensions in June 2018. This collimator mitigated the background from kaon decays upstream of the last GTK station (upstream background) entering the FV through the aperture of the last dipole of the beam achromat. An increase of signal acceptance is achieved while retaining a good separation of $K^+ \to \pi^+\nu\bar{\nu}$ decays from upstream background. The new collimator allows removing the restrictions on the extrapolated position of the π^+ track at

a plane transverse to the beam direction at the beginning of the FV present in the 2016 and 2017 analyses. In addition, a BDT algorithm is exploited using as inputs the track angles, extrapolated positions of the π^+ at the beginning of the FV and the decay vertex position.

The S2 sample is divided into 6 categories defined by 5 GeV/c-wide momentum bins from 15 to 45 GeV/c. A separate selection is applied to each category to achieve optimal signal sensitivity. The lower statistics of S1 sample do not allow significant sensitivity improvements if divided in momentum bins and is treated as a separate category integrated over momentum.

The Single Event Sensitivity ($S.E.S.$) for a SM $K^+ \to \pi^+\nu\bar{\nu}$ decay with the full 2018 data set, integrated over all categories, is

$$S.E.S. = (1.11 \pm 0.07) \times 10^{-11}, \tag{2}$$

which corresponds to $N_{\pi\nu\bar{\nu}}^{expected} = 7.58 \pm 0.40_{syst} \pm 0.75_{ext}$. The signal expectation is normalized to $K^+ \to \pi^+\pi^0$ decays selected similarly to $K^+ \to \pi^+\nu\bar{\nu}$, but without photon and multi-charged particle rejection applied in the region $0.010 < m^2_{\rm miss} < 0.026$. The statistical uncertainty on the $S.E.S.$ is negligible. The systematic uncertainty receives the main contributions from: trigger efficiency; random veto losses induced by the photon and multi-charged particle rejection procedure; simulation of the π^+ losses due to interactions in the detector material upstream of the hodoscopes. Contribution from background contamination inside the normalization region and instantaneous intensity are sub-dominant. The external uncertainty is due to the theoretical knowledge of the $K^+ \to \pi^+\nu\bar{\nu}$ branching ratio.

The background contamination is $N_{bg} = 5.28^{+0.99}_{-0.74}$ events, composed of K^+ decays (1.98 ± 0.15 events) and upstream background ($3.30^{0.98}_{-0.73}$ events). The main contribution to the K^+ decay background is from $K^+ \to \pi^+\pi^0(\gamma)$, $K^+ \to \mu^+\nu(\gamma)$, $K^+ \to \pi^+\pi^-e^+\nu$ and $K^+ \to \pi^+\pi^+\pi^-$ decays in this order. The background predictions are validated in dedicated background validation regions (see Figure 2) for $K^+ \to \pi^+\pi^0(\gamma)$, $K^+ \to \mu^+\nu(\gamma)$ and $K^+ \to \pi^+\pi^+\pi^-$. Upstream and $K^+ \to \pi^+\pi^-e^+\nu$ background predictions are validated using separate samples statistically independent to the $K^+ \to \pi^+\nu\bar{\nu}$ selection, as explained in the caption of Figure 3.

4. Results

After unmasking the signal regions, thirteen events are found in Region 1 and four in Region 2, as shown in Figure 4, left.

In total, adding the result of the $K^+ \to \pi^+\nu\bar{\nu}$ analysis performed on the 2016 [10], 2017 [11] and 2018 data, NA62 has observed 20 candidate events in the signal regions.

The data is separated in categories depending on momentum and hardware configuration, as described in the caption of Figure 4, right. A maximum likelihood fit is performed with the $K^+ \to \pi^+\nu\bar{\nu}$ branching ratio as a fit parameter. The uncertainties on the background and signal estimates are used as nuisance parameters in the fit. The resulting branching ratio is

$$BR(K^+ \to \pi^+\nu\bar{\nu}) = (11.0^{+4.0}_{-3.5} \pm 0.3) \times 10^{-11} \text{ @ } 68\% \text{ CL}, \tag{3}$$

compatible with the SM value within one standard deviation. The first uncertainty is statistical, dominated by the Poissonian fluctuation of the expected background, and the second is systematic,

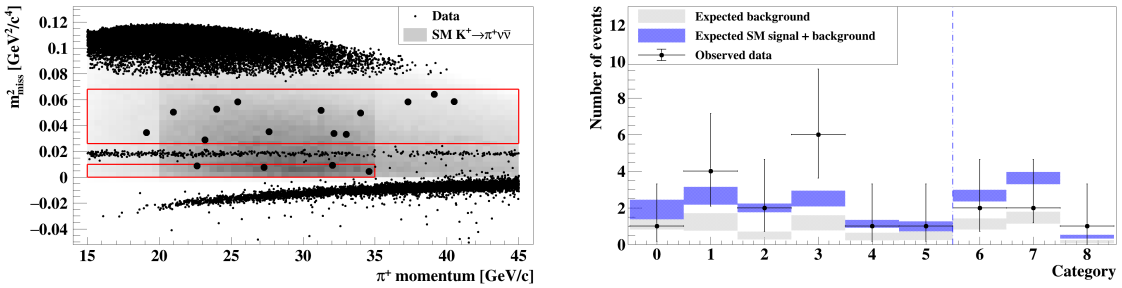

Figure 4: Left: Reconstructed $m^2_{\rm miss}$ as a function of π^+ momentum satisfying the $K^+ \to \pi^+\nu\bar{\nu}$ selection criteria. The grey area corresponds to the expected distribution of $K^+ \to \pi^+\nu\bar{\nu}$ MC events. The two boxes define the signal regions. The events observed in R1 and R2 are shown together with the events found in the background and validation regions. **Right:** Comparison between the expected and observed number of events in the different categories used in the maximum likelihood fit to extract the $K^+ \to \pi^+\nu\bar{\nu}$ branching ratio. Categories 0 to 5 correspond to the six 5 GeV/c-wide momentum bins of S2. Category 6,7 and 8 correspond to S1, 2017 and 2016, respectively. The observed data for each category is indicated by the black dots. The grey boxes show the expected number of background events with the corresponding uncertainty. The blue shaded rectangles indicate the expected number of events summing the background contribution and a SM signal with its uncertainty.

resulting from the uncertainty of the signal expectation. The statistical significance of the signal is 3.5 standard deviations, estimated using the CLs method [12]. This is the most precise determination of the $K^+ \to \pi^+\nu\bar{\nu}$ process to date and the first unambiguous evidence for the existence of this extremely rare process.

References

[1] M. Blanke, A. J. Buras, B. Duiling, K. Gemmler , S. Gori, *JHEP* **903**, 108 (2009)

[2] A. J. Buras, D. Buttazzo, R. Knegjens, *JHEP* **1511**, 166 (2015)

[3] T. Blazek, P. Matak, *Int. J. Mod. Phys.* A **29.no.27**, 1450162 (2014)

[4] J. Isidori et al., *JHEP* **0608**, 064 (2006)

[5] M. Blanke, A. J. Buras, S. Recksiegel, *Eur. Phys. J.* C **76.no.4**, 182 (2016)

[6] J. Isidori, M. Bordone, D. Buttazzo, J. Monnard, *Eur. Phys. J.* C **77**, 618 (2017)

[7] A. J. Buras, D.Buttazzo, K.Girrbach-Noe, R. Knegjens, *JHEP* **11**, 033 (2015)

[8] J. Brod, M. Gorbahn, E. Stammou, *Phys. Rev.* D **83**, 034030 (2011)

[9] The NA62 Collaboration, *JINST* **12**, P05025 (2017)

[10] The NA62 Collaboration, *Phys. Lett.* B **791**, 156-166 (2019)

[11] The NA62 Collaboration, *JHEP* **11**, 042 (2020)

[12] A.L. Read, J. Phys. **G28**, 2693 (2002)